

Fig. 3. Laue photograph of 1.5-cm thick potassium single crystal with appreciable orientation spread; 125 kv, 5 ma, 20 minutes, 10 cm between slit and film.

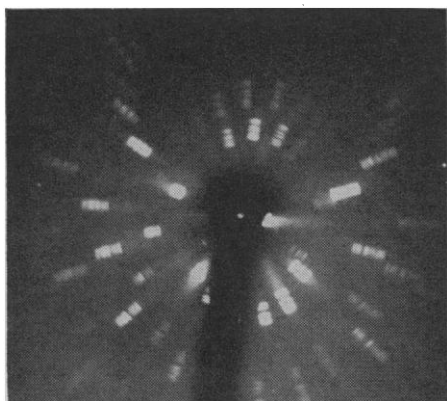


Fig. 4. Laue photograph of a 2-cm thick aluminum crystal grown by a Bridgman technique; 150 kv, 5 ma, 15 minutes, 10 cm between slit and film.

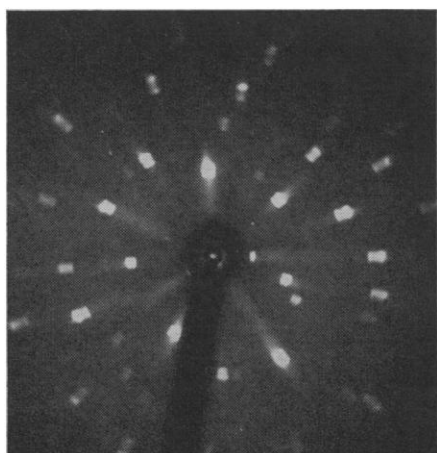


Fig. 5. Laue photograph of a 9 mm thick strain-annealed aluminum crystal; 150 kv, 5 ma, 5 minutes, 10 cm between slit and film.

ness of the crystal, is illustrated in Fig. 2, which shows a Laue photograph of a thick (2 cm) aluminum crystal. The crystal thickness in this instance is not negligible compared with its distance from the photographic film. The diffraction "spots" are therefore produced as radial streaks of length equal to the projected thickness of the crystal (2, 3), the direction of projection being parallel to the diffracted rays, and the plane of projection being the photographic film.

Appreciable misorientation within an apparently single crystal is recognized in the Laue photograph of a potassium crystal (Fig. 3). The streaks are longer than can be explained by the geometric effect discussed above, and their length is not simply related to the angle of diffraction. The detail in the individual streaks indicates the presence of subcrystals with large orientation spread. We have not ascertained whether the crystals grow imperfectly or whether they become deformed by handling.

The x-ray Laue photograph (Fig. 4) of an aluminum single crystal (2 cm thick) grown by the Bridgman method shows streaks of the predicted length for a nearly perfect crystal, so that considerable misorientation in subcrystals is excluded. However, there is detail along the streaks, presumably due to slightly misset mosaic "blocks" failing to produce streak intensity at one point and increasing it in another. The somewhat periodic fluctuation of intensity along the streaks at first seems surprising.

A very similar periodic structure in small crystals has been described by Guinier (6). Strain-annealed aluminum (7) does not show the intensity fluctuation to the same extent (Fig. 5). The increase in intensity at the ends of the streaks is a coherence effect (2) and corresponds to the predictions made by Kato (8) from the dynamic theory of x-ray diffraction for crystals of low absorbing power. Murdock (9) has previously observed the effect, but his explanation needs modifications in the light of more recent dynamic theory.

The high-voltage Laue technique may be applied to the study of the influence of impurities on the crystal diffraction. Primary extinction reduces the intensities of reflections of ammonium dihydrogen phosphate (ADP) crystals of high perfection. By contamination with Cr^{3+} ions, the perfection of the crystals is reduced and the

Table 1. Approximate integrated intensities of recorded Laue diffractions from section of an ammonium dihydrogen phosphate (ADP) crystal containing pure and chromium-contaminated portions (90 kv, 5 ma, 25 minutes, 20 cm between slit and film).

hkl	Intensities* (summed over all orders)	
	Pure ADP	Cr^{3+} -contaminated ADP
541	6.8	14.3
631	11.8	19.2

* Fluctuations between symmetrically equivalent spots (due to lack of precision in orientation, and other effects) range about ± 25 percent from the mean.

intensities are correspondingly increased (Table 1). As is typical for primary extinction, the weak diffractions are not affected.

B. PARETZKIN
H. STEFFEN PEISER

National Bureau of Standards,
Washington 25, D.C.

References and Notes

1. G. Bacon, *Neutron Diffraction* (Clarendon Press, Oxford, ed. 2, 1962).
2. H. S. Peiser and E. P. Levine, *Advan. X-Ray Anal.* 6, 158 (1963).
3. J. M. Cork, *Phys. Rev.* 42, 749 (1932).
4. H. S. Peiser and J. R. Rait, *Acta Cryst.* 8, 738 (1955).
5. A. Guinier and J. Tennevin, *ibid.* 2, 133 (1949).
6. A. Guinier, *Imperfections in Nearly Perfect Crystals* (Wiley, New York, 1952), p. 402.
7. J. M. Frankland, thesis, Univ. of London (1931).
8. N. Kato, *Acta Cryst.* 13, 349 (1960).
9. C. C. Murdock, *Phys. Rev.* 45, 117 (1934).
10. We thank J. M. Frankland, A. T. Horton, A. F. Hoyte, T. H. Orem, and J. L. Torgesen for allowing use of their crystals.

8 July 1964

Crystal and Molecular Structure of Ferrichrome A

Abstract. *The crystal structure of ferrichrome A ($\text{C}_{11}\text{H}_{18}\text{N}_3\text{O}_{20}\text{Fe}\cdot 4\text{H}_2\text{O}$) has been determined by x-ray diffraction. The amino acid sequence in the hexapeptide ring is confirmed to be -Orn-Orn-Orn-Ser-Ser-Gly-, and the conformation of this ring is trans at each peptide linkage. The absolute configuration of the three hydroxamate rings at the iron atom is that of a left-handed propeller. Disorder is found concerning the positions of some of the side chains and one of the four water molecules.*

Ferrichrome A, a product of the metabolism of the smut fungus *Ustilago sphaerogena*, is a ferric hydroxamate and a cyclic hexapeptide consisting of residues of the amino acids glycine, serine, and ornithine (1). It is related

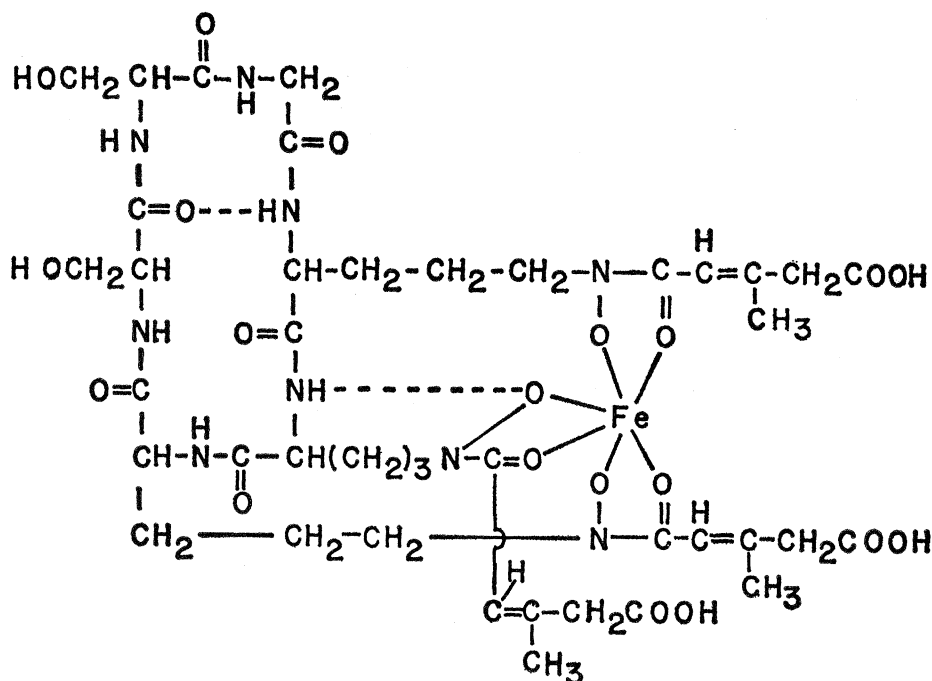


Fig. 1. Ferrichrome A.

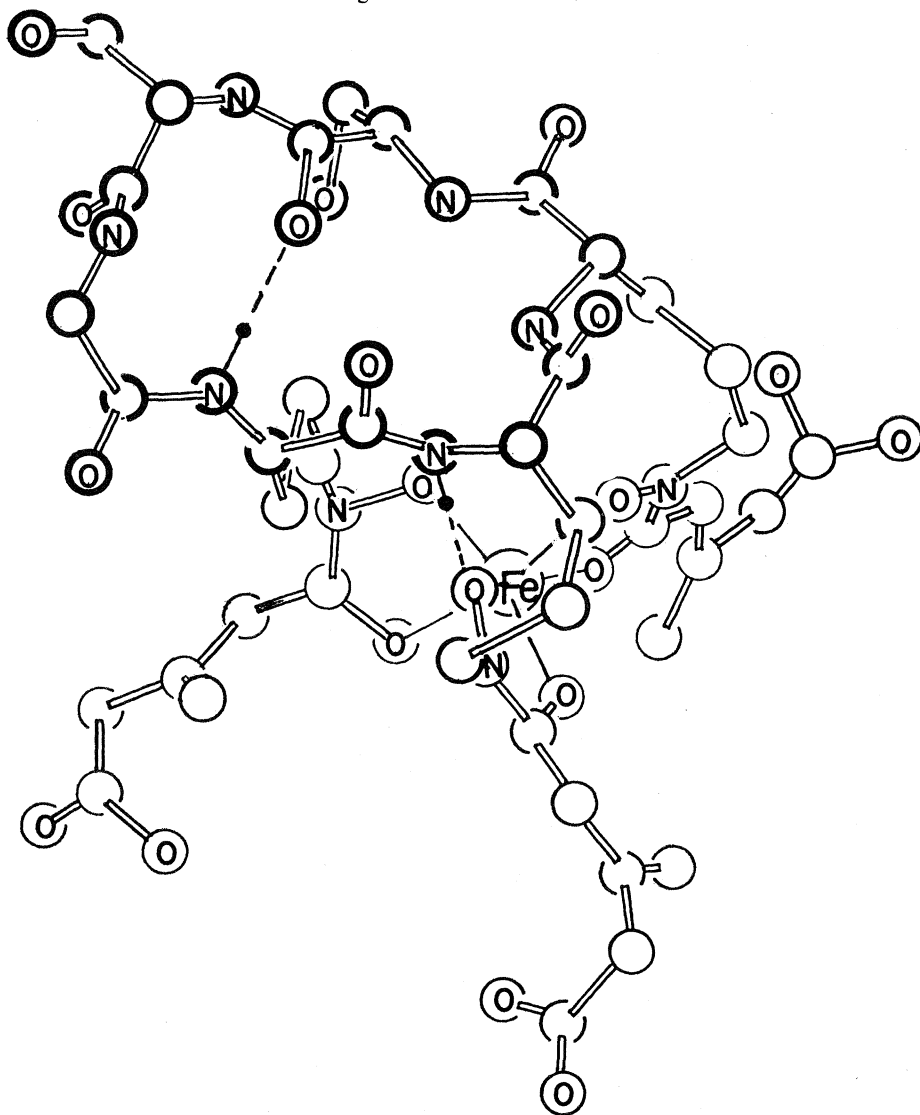


Fig. 2. Molecular shape of ferrichrome A; only one conformation is shown for the disordered atoms, which are the oxygen at the upper left corner, the carboxyl at the far right, and the center of the methyl glutaconic acid residue at the lower left.

in structure to several substances which are growth factors for certain microorganisms (2-4). Its structure is also of interest for possible clues to the structures of proteins. By x-ray diffraction methods we have determined the crystal structure and have found the molecular structure (Fig. 1) to be in agreement with deductions from chemical evidence (1, 5).

Crystals of composition $C_{41}H_{88}N_9O_{20} \cdot Fe \cdot 4H_2O$ are monoclinic, space group $P2_1$, with $a = 11.02 \pm 0.02$, $b = 13.26 \pm 0.03$, $c = 18.22 \pm 0.01$ Å, $\beta = 99.48^\circ$, $Z = 2$. The density calculated from the x-ray data, 1.42 ± 0.01 , is to be compared with the measured value 1.45 ± 0.06 g/ml (2). Diffraction measurements were made by scintillation counting with a crystal measuring about 0.1 by 0.1 by 0.2 mm. Because $MoK\alpha$ radiation gave low counting rates, we recorded the intensities of 3115 independent reflections with $FeK\alpha$ radiation. Of these, only 56 were recorded as zero. To determine the absolute configuration of the structure we measured the intensities of 71 pairs (hkl and $h\bar{k}l$) with $CuK\alpha$ radiation, which iron atoms scatter with a large phase shift (anomalous dispersion effect). Significant intensity differences were observed for 40 pairs, and in each case the sign of the difference is explained by our final structure. This test shows that we have the correct absolute configuration and at the same time is strong evidence for the correctness of the structure we have determined.

The position of the iron atom was guessed correctly from the Patterson function and later confirmed with the anomalous dispersion data. A superposition of the Patterson function with the Fe-Fe vector as the shift vector suggested positions for the six oxygen neighbors of iron and for several other atoms. The rest of the structure was determined by repeated electron-density calculations alternated with least-squares refinement.

The discrepancy index

$$R = \frac{\sum ||F_o| - |F_c||}{\sum |F_o|}$$

was reduced to 0.14 with 75 atoms in the structure. The electron density maps were excellent for most of the structure but suggested disorder for a few atoms. With some atoms distributed at random between alternate sets of positions, R was reduced to 0.11. One water molecule was distributed among three sites so close together that only one at

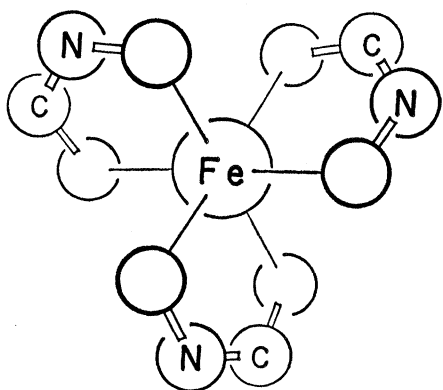


Fig. 3. Absolute configuration around the iron atom.

a time could be occupied. The oxygen atom of one serine side chain, the methyl carbon and α -carbon of one methyl glutamic acid residue, and the oxygen atoms of the terminal carboxyl group of another glutamic acid were each assigned two sites corresponding to two ways of twisting each of these groups. An electron-density-difference function calculated at this point showed peaks which can be explained as the result of either anisotropic thermal motion or slight shifts associated with the disorder of neighboring atoms. Other peaks were found in correct positions for about 40 hydrogen atoms on those parts of the structure for which the effects of disorder and anisotropic motion are less severe. Further calculations taking account of these hydrogen atoms and some of the anisotropic motion effects have reduced R to 0.09.

The molecular shape is shown in Fig. 2. The sequence of amino acid residues (ornithine, serine, and glycine) in the cyclic peptide is -Orn-Orn-Orn-Ser-Ser-Gly-. The conformation of the ring is *trans* at each peptide linkage. The absolute configuration of each of the five asymmetric α -carbon atoms is the same as that commonly found in other peptides of biological origin and is described conventionally as left-handed. The absolute configuration of the three hydroxamate rings at the iron atom (Fig. 3) is that of a left-handed propeller. In such a ring structure there are two distinct ways in which the polarities of the C—N bonds can be arranged, either all the same way or one different from the other two. We find the more symmetrical structure in which the polarities are the same in the three rings, as shown in Fig. 3.

We recognize two hydrogen bonds within the molecule. One of length 2.99 Å bridges the peptide ring and joins the α -nitrogen of one ornithine

residue to the carbonyl oxygen of one serine residue. This bond distance corresponds to a weak bond. In the flat representation of this ring (Fig. 1) there seems to be the possibility of a second hydrogen bond across the ring, but the folding of the ring in the actual structure does not permit this. A second hydrogen bond of length 2.79 Å joins the α -nitrogen of the second ornithine residue to the oxygen atom of the δ -nitrogen of this same residue.

Several other hydrogen bonds connect various oxygen atoms with water molecules which in turn are connected to other ferrichrome molecules. There is disorder in some of these bonds, because they involve some of the atoms with alternate sites.

Bond distances and angles which do not involve hydrogen atoms are in good agreement with the expected values, with standard deviations of the dis-

tances being approximately 0.02 Å. The six oxygen neighbors of the iron atom are at distances ranging from 1.96 to 2.07 Å. The bond angles at the iron atom which would be 90° for a regular octahedron range from 78° to 101°.

ALLAN ZALKIN
J. D. FORRESTER
DAVID H. TEMPLETON

Department of Chemistry and
Lawrence Radiation Laboratory,
University of California, Berkeley

References and Notes

1. T. Emery and J. B. Neilands, *J. Am. Chem. Soc.* **83**, 1626 (1961).
2. J. B. Neilands, *Bacteriol. Rev.* **21**, 101 (1957).
3. V. Prelog, *Pure Appl. Chem.* **6**, 327 (1963).
4. O. Mikeš and J. Turková, *Chem. Listy* **58**, 65 (1964).
5. S. J. Rogers, R. A. J. Warren, J. B. Neilands, *Nature* **200**, 167 (1963).
6. We thank Prof. J. B. Neilands for providing the crystals for this investigation and for helpful discussions concerning the molecular structure. This work was done under the auspices of the AEC.

6 July 1964

Sodium Perxenate and Xenon (II) Difluoride Reduction at the Dropping-Mercury Electrode

Abstract. *Sodium perxenate in alkaline solutions is reduced in a single step to xenon at the dropping-mercury electrode. The half-wave potential for perxenate changes from -0.21 to -0.31 volts against a Hg_2SO_4 -Hg reference electrode in the pH range 10.1 to 11.3. Xenon (II) difluoride in acidic solution is reduced in a single step to xenon, at the potential of approximately zero against the Hg_2SO_4 -Hg reference electrode. The reduction wave is followed by a broad maximum which can be effectively suppressed by fluoride ion. The diffusion current varies in linear fashion with concentration.*

Investigation of perxenate and xenon (II) difluoride reduction at the dropping-mercury electrode was undertaken to learn whether these compounds are

reduced directly to xenon, as has been observed for the xenic acid by Jaselskis (1), or whether perxenate undergoes a stepwise reduction.

Table 1. Polarographic characteristics of sodium perxenate and xenon (II) difluoride. The pH is that of the supporting electrolyte; abbreviations are: i , diffusion current; C , concentration of xenon compound; m , mass of flow of mercury (mg/sec); and t is drop time (sec).

Concn (10 ⁻⁶ M)	pH	$E_{1/2}$ vs Hg_2SO_4 -Hg (v)	i (μ a)	$i/Cm^{1/2}t$
<i>Xenic acid</i>				
9.1	6.4*	-0.32	1.06	7.71
<i>Sodium perxenate</i>				
14.1	11.3†	-.31	2.10	9.86
14.1	10.1‡	-.21	2.05	9.63
14.1	3.0+§	.0	1.56	7.33
17.1	11.3†	-.31	2.55	9.93
17.1	3.0+§	.0	1.90	7.40
<i>Xenon (II) difluoride</i>				
17.3	4.5‡	.0	0.58	2.23
34.7	4.5‡	.0	1.25	2.40
69.5	4.5‡	.0	2.55	2.44

* Unbuffered 0.1M potassium sulfate. † 0.1M potassium sulfate and 0.001M sodium hydroxide. ‡ 0.1M potassium sulfate and 0.005M sodium carbonate and bicarbonate. § Acidified solution of sodium perxenate in 0.1M potassium sulfate. || 0.1M potassium sulfate, 0.02M acetic acid, and 0.02M sodium acetate or 0.1M potassium sulfate, 0.02M acetic acid, 0.02M sodium acetate, and 0.1M sodium fluoride.